

Controllable Egocentric Video Generation via Occlusion-Aware Sparse 3D Hand Joints

Chenyanguang Zhang^{*1}, Botao Ye^{*1}, Boqi Chen^{*1}, Alexandros Delitzas^{1,2},
Fangjinhua Wang¹, Marc Pollefeys^{1,3}, and Xi Wang¹ *

¹ ETH Zurich

² MPI for Informatics

³ Microsoft

Abstract. Motion-controllable video generation is crucial for egocentric applications in virtual reality and embodied AI. However, existing methods often struggle to achieve 3D-consistent fine-grained hand articulation. By adopting on 2D trajectories or implicit poses, they collapse 3D geometry into spatially ambiguous signals or over rely on human-centric priors. Under severe egocentric occlusions, this causes motion inconsistencies and hallucinated artifacts, as well as preventing cross-embodiment generalization to robotic hands. To address these limitations, we propose a novel framework that generates egocentric videos from a single reference frame, leveraging sparse 3D hand joints as embodiment-agnostic control signals with clear semantic and geometric structures. We introduce an efficient control module that resolves occlusion ambiguities while fully preserving 3D information. Specifically, it extracts occlusion-aware features from the source reference frame by penalizing unreliable visual signals from hidden joints, and employs a 3D-based weighting mechanism to robustly handle dynamically occluded target joints during motion propagation. Concurrently, the module directly injects 3D geometric embeddings into the latent space to strictly enforce structural consistency. To facilitate robust training and evaluation, we develop an automated annotation pipeline that yields over one million high-quality egocentric video clips paired with precise hand trajectories. Additionally, we register humanoid kinematic and camera data to construct a cross-embodiment benchmark. Extensive experiments demonstrate that our approach significantly outperforms state-of-the-art baselines, generating high-fidelity egocentric videos with realistic interactions and exhibiting exceptional cross-embodiment generalization to robotic hands.

Keywords: Egocentric Vision · Hand Control · Video Generation

1 Introduction

The recent advance of generative models has revolutionized video synthesis, enabling high-fidelity content creation [1, 4, 21, 46, 56]. Beyond passive gener-

* * Authors with equal contributions.

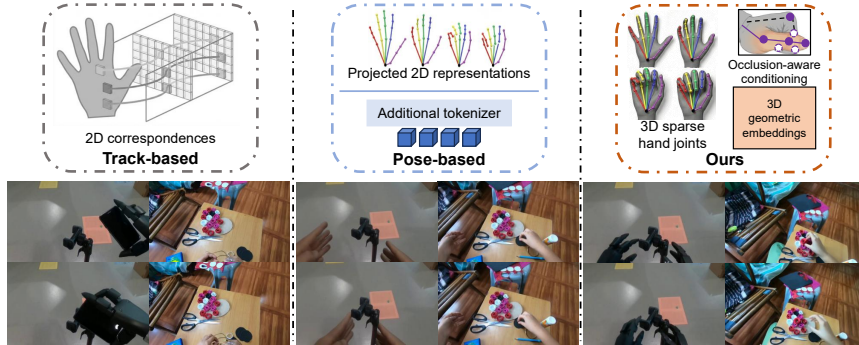


Fig. 1: Comparison with existing controllable video generation methods. We leverage sparse 3D hand joints as a cross-embodiment control signal, enabled by our occlusion-aware conditioning and 3D geometric embeddings. Consequently, our method generates high-fidelity consistent hands that align with complex input motions under severe occlusion. In contrast, pose-based methods struggle to generalize across diverse embodiments, and track-based methods exhibit weak spatial control.

ation, recent research increasingly focuses on motion-controlled video synthesis, aiming to grant users precise authority over spatial and temporal dynamics [6, 10, 23, 43, 55]. Such controllability is particularly critical in egocentric scenarios, where fine-grained hand-object interactions dominate the visual field and determine perceptual realism.

Controlling egocentric video generation is substantially more challenging than general motion synthesis. The model must simultaneously preserve high-frequency articulation details, maintain geometric plausibility under frequent occlusion, and follow user-specified trajectories with strict spatial consistency. However, existing control paradigms struggle to satisfy these requirements. Track-based methods [6, 11, 43, 59, 61] treat motion flows as isolated 2D point trajectories, discarding the rigid structural integrity of the hand and inherently lacking depth awareness, resulting in unrealistic motion details when facing complex interactions. Pose-based methods [24, 33] represent hand motion using implicit pose signals and generally follow two strategies. One encodes poses into compressed, low-frequency latent manifolds [33, 44], which smooths fine-grained articulation details and thus weakens the high-frequency spatial cues required by generators, often producing temporally averaged or floaty motion artifacts [14, 24, 63, 64]. The other projects poses into 2D skeletal maps or masks [24, 32]. Although interpretable, such projections collapse 3D geometry into ambiguous 2D signals, creating visual clutter and ambiguous ordering cues that hinder precise control. Moreover, because the pose representation is inherently latent and relies heavily on rigid, human-centric kinematic priors, it precludes intuitive interactive editing and lacks cross-embodiment generalization to diverse robotic hands.

Our insight is that sparse 3D hand joints offer a more suitable control signal for egocentric video generation by providing: (1) explicit 3D geometry to resolve

occlusion ambiguities, (2) distinct semantic identities for each articulation, (3) a sparse and intuitive interface for user manipulation, and (4) an embodiment-agnostic representation for seamless cross-embodiment generalization. Specifically, unlike skeletal maps or latent pose codes that embed rigid, human-specific kinematic assumptions, sparse 3D joints represent articulation as unconstrained spatial coordinates. This inherent flexibility makes the control signal naturally transferable across the diverse structural topologies of humanoids and robotic hands [36, 60]. Consequently, our control paradigm not only enhances human egocentric video fidelity but is also demonstrated to be effective for robotic dexterous manipulation without requiring complex domain adaptation.

However, directly injecting 3D joints into an egocentric image-to-video generation model is non-trivial and introduces two fundamental challenges. **First, occlusion ambiguity.** Egocentric interactions involve severe and dynamic mutual occlusions between fingers and objects. The model must explicitly reason about visibility states to avoid feature contamination and trajectory conflicts. This challenge comes in two forms. (1) *Source occlusion*: in the reference frame, occluded joints should not contribute unreliable visual features. Otherwise, hidden articulations may inherit incorrect textures, leading to hallucinations when later revealed. (2) *Target occlusion*: during motion propagation, foreground fingers frequently cross over background ones. Without 3D-aware conditioning, features may be incorrectly assigned across layers, producing anatomical artifacts such as merged or intersecting fingers. **Second, preservation of 3D structure.** A naive conditioning strategy that projects 3D joints into 2D feature space discards depth and structural priors, undermining the key advantage of 3D control. To achieve high-fidelity generation, semantic identity and geometric relationships must be incorporated directly into the generation process.

To address these challenges, we propose a novel occlusion-aware, geometry-preserving control framework for egocentric image-to-video generation (Figure 1). First, we construct occlusion-aware motion condition features by explicitly modeling both source and target occlusion. In the source reference frame, we sample latent VAE features by aggregating local visual contexts around each joint, while filtering out unreliable signals via an occlusion penalty strategy. Then, these refined features are propagated to target frames along the 3D hand joint trajectories. To handle dynamic target occlusions during motion, we introduce a 3D-based weighting mechanism that adaptively adjusts feature contributions of the joints, ensuring robust motion feature conditioning during severe mutual occlusion. Finally, to fully exploit the semantic and geometric richness of sparse hand joints in the generation process, we construct 3D geometric embeddings incorporating both 3D coordinate information and learnable semantic indices. Despite explicitly modeling occlusion and 3D geometry, the entire control module remains lightweight and minimally perturbs the pretrained latent space, allowing efficient integration with modern video generation backbones.

Furthermore, we observe a lack of large-scale benchmarks for training and evaluating controllable egocentric video generation models with accurate 3D hand trajectories across both human and robotic domains. To bridge this gap,

we develop an automated annotation and filtering pipeline. For human interactions, we leverage the Ego4D dataset [12] to produce over *one million* high-quality video clips with precise hand trajectories. To support cross-embodiment research, we extend this pipeline to project offline robot kinematics from Humanoid Everyday [66] into the visual plane, curating a robotic benchmark comprising thousands of motion-aligned clips across diverse humanoid hands. Extensive experiments on Ego4D, EgoDex [17], and Humanoid Everyday demonstrate that our method outperforms existing approaches. It achieves superior accuracy in controlling egocentric motions under heavy occlusion and exhibits robust cross-embodiment generalization. Moreover, our framework uniquely enables interactive, fine-grained micro-manipulation, allowing users to control articulations down to the isolated movement of a single joint.

2 Related Works

Video Generation Models. Early advances in video generation were primarily driven by Latent Diffusion Models [39] (*e.g.*, 3D U-Net [4]) to maintain spatial-temporal coherence. More recently, the field has undergone a paradigm shift toward Diffusion Transformers (DiTs) [34], which leverage the scalability of transformer backbones to handle long-range temporal dependencies. State-of-the-art open-source models such as WAN [46] and HunyuanVideo [22] have significantly narrowed the quality gap between open and proprietary systems with exceptional photorealistic detail. Despite their impressive generative priors, these DiT-based models lack the mechanisms for precise, fine-grained control over local dynamics. Our work provides concise, 3D-aware control using sparse hand joints as explicit signals to guide complex egocentric video generation.

Motion Control in Video Generation. Early explorations into motion-controlled video generation focused on training-free methods [19,28,30,37], which optimize input noisy latents or manipulate attention mechanisms to achieve zero-shot guidance. Subsequently, finetuning-based approaches have become the dominant paradigm [5,7,11,15,25,26,42,49–51,55,58,65,67], using auxiliary adapters to inject various motion signals into the base model. Among various control modalities, point tracks have emerged as a unified representation for guiding general motions [11,42,47,55,57,59,61,65]. Most recently, state-of-the-art methods such as Wan-Move [6] and MotionStream [43] have advanced this paradigm by injecting 2D point trajectories directly into the latent space to provide motion context. Despite their general success, 2D-track-based methods discard the structural integrity and 3D-awareness essential for egocentric interactions, often failing to resolve severe occlusions and causing structural hallucinations. To overcome this, our method leverages sparse 3D hand joints, explicitly tackling the inherent challenges of 3D-to-2D information loss through occlusion-aware conditioning and 3D geometric embeddings.

Egocentric World Models. Rapid advances in video generation have catalyzed the development of egocentric world models that simulate first-person dynamics to facilitate applications in Virtual Reality (VR) and Robotics. A prominent line

of research focuses on synthesizing egocentric content that depicts a variety of controlled human behaviors, by conditioning generative priors on modalities of human poses, trajectories, and action signals [2, 15, 33, 44, 48, 52, 53, 62, 64]. Building upon these human-centric simulations, a parallel body of work seeks to bridge the embodiment gap for the robotics community [3, 8, 9, 13, 20, 27, 29, 31, 41]. While existing methods successfully capture holistic dynamics, they often lack the fine-grained kinematic fidelity required to simulate dexterous interactions. Our method integrates precise 3D control into generative models via embodiment-agnostic sparse joints, achieving seamless cross-embodiment generalization.

3 Method

3.1 Preliminaries: Video Generation Model

Our method builds upon the WAN framework [46], which formulates video generation as a continuous-time conditional flow matching problem. Flow matching models the generative process as a deterministic Ordinary Differential Equation (ODE) that transports samples from a simple prior distribution toward the data distribution. Let $x_1 \sim p_{\text{video}}$ denote the latent representation of a real video encoded by a 3D-VAE, and let $x_0 \sim \mathcal{N}(0, I)$ be Gaussian noise sampled from the prior distribution. A conditional probability path is defined by linear interpolation between x_0 and x_1 : $x_t = (1 - t)x_0 + tx_1, t \in [0, 1]$. The time derivative of this path is constant and is given by $\frac{dx_t}{dt} = x_1 - x_0$.

A time-conditioned neural network $v_\theta(x_t, t, c)$, parameterized as a DiT conditioned on multimodal context c (e.g., texts, reference images, or control signals), is trained to approximate this target velocity field with the objective:

$$\mathcal{L} = \mathbb{E}_{t \sim \mathcal{U}(0,1), x_0, x_1, c} \left[\|v_\theta(x_t, t, c) - (x_1 - x_0)\|^2 \right]. \quad (1)$$

At inference time, video samples are generated by solving the learned ODE $\frac{dx_t}{dt} = v_\theta(x_t, t, c)$, from $t = 0$ to $t = 1$ using a numerical ODE solver, thereby transporting the prior sample to the video data manifold.

The standard WAN framework conditions the velocity field v_θ in a global context, which is insufficient to define precise dexterous manipulations. Our work focuses on fine-grained motion control for egocentric video generation by introducing sparse 3D hand joints $\mathbf{J} \in \mathbb{R}^{F \times N \times 3}$ as an explicit motion guide.

3.2 Occlusion-Aware 3D Hand Motion Control

Our framework (Figure 2) integrates sparse 3D hand joints into the image-to-video generation process by addressing two specific challenges of egocentric interactions. First, to resolve the ambiguity of mutual occlusions, we devise an occlusion-aware motion conditioning strategy. This involves a two-stage process: (1) Occlusion-removed context aggregation in the source reference frame to prevent feature contamination from occluding parts, and (2) Occlusion-aware

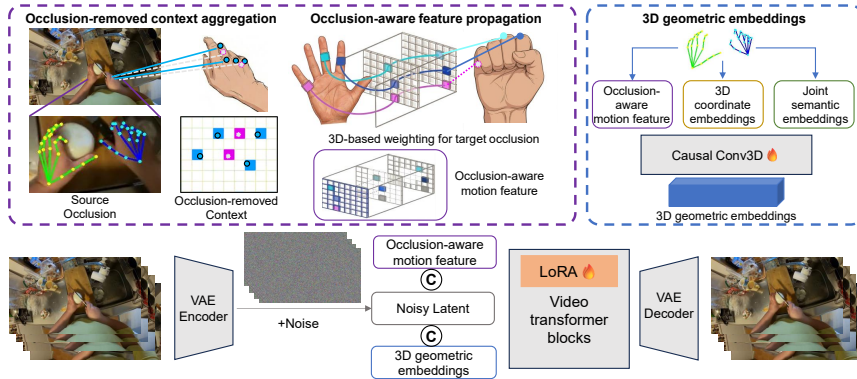


Fig. 2: Method overview. Our framework uses sparse 3D hand joints to represent motions by constructing two embedding streams. The occlusion-aware motion feature is yielded by first penalizing occluded regions to extract reliable context from the source frame, and then propagating it with modulating 3D-aware feature weights to handle target occlusion. The 3D geometric embedding is formed by processing this motion feature along with 3D joint coordinates and semantic embeddings through a Causal Conv3D block. Finally, both embeddings are concatenated with the noisy latent and fed into LoRA-adapted DiT blocks.

feature propagation to modulate feature influence during target frame generation. Second, to fully leverage the spatial richness of the 3D joints, we align 3D geometric embeddings directly into the video latent space, encoding both articulation semantics and 3D consistency.

Occlusion-Removed Context Aggregation. To guide the generation of subsequent frames, we first aim to extract visual context features from the VAE latent of the source image corresponding to each hand joint. However, two obstacles prevent simple feature sampling, *i.e.*, *sparsity* and *source occlusion*.

Unlike track-based methods [6, 43] that rely on dense point grids for better performance [6], hand joints are inherently sparse ($N \leq 42$). Relying solely on single-pixel features at projected coordinates captures insufficient context for complex hand-object interactions. To address this, we aggregate local features by modeling the spatial influence of each joint. Given the set of 3D hand joints $\mathcal{J}_{src} = \{\mathbf{J}_i\}_{i=1}^N$ in the source camera frame, we project them to 2D coordinates and disparity (inverse depth) maps $\mathbf{u}_i, d_i = \Pi(\mathbf{J}_i, \mathbf{K})$ using camera intrinsic \mathbf{K} . We then generate a localized Gaussian heatmap $\mathbf{M}_i(\mathbf{x}) = \exp\left(-\frac{\|\mathbf{x}-\mathbf{u}_i\|_2^2}{2\sigma^2}\right) \in \mathbb{R}^{H \times W}$ at a grid location $\mathbf{x} \in \mathbb{R}^2$ for each joint i , where σ controls the spatial bandwidth, defining the receptive field for context aggregation.

While this Gaussian pooling captures context, it introduces a risk of feature contamination under self-occlusion. For instance, if a thumb occludes an index finger in the source view, naive aggregation around the index finger’s projected position would erroneously sample the thumb’s texture. Using this contaminated feature to generate the index finger in later frames would lead to severe halluci-

nations. To resolve this, we define a pairwise occlusion penalty $P_{i \leftarrow j}$ representing the likelihood that joint j occludes joint i :

$$P_{i \leftarrow j} = \underbrace{\exp\left(-\frac{\|\mathbf{u}_i - \mathbf{u}_j\|_2^2}{2\tau^2}\right)}_{\text{Spatial Overlap}} \cdot \underbrace{\sigma(\gamma(d_j - d_i))}_{\text{Depth Ordering}}, \quad (2)$$

where $\sigma(\cdot)$ is the sigmoid function. The term $\sigma(\gamma(d_j - d_i))$ approaches 1 when the joint j is significantly closer to the camera than the joint i ($d_j > d_i$), indicating a high probability of occlusion.

Finally, we extract the purified context feature \mathbf{f}_i from the source latent map \mathcal{Z}_0 . We apply a gated average pooling of features by:

$$\mathbf{f}_i = (1 - \max_{j \neq i} P_{i \leftarrow j}) \cdot \sum_{\mathbf{x}} \left(\frac{\mathbf{M}_i(\mathbf{x})}{\sum_{\mathbf{x}'} \mathbf{M}_i(\mathbf{x}') + \epsilon} \cdot \mathcal{Z}_0(\mathbf{x}) \right). \quad (3)$$

This operation effectively filters the signal: if a joint is occluded (with visibility $1 - \max_{j \neq i} P_{i \leftarrow j} \approx 0$), its contribution to the feature is suppressed, preventing the propagation of erroneous texture information.

Occlusion-Aware Feature Propagation. Once the clean source features \mathbf{f}_i are extracted, the next challenge is how to propagate them to the target frames $t \in \{1, \dots, T\}$ along the trajectories of the 3D hand joints, to provide the generation process with accurate motion guidance. A naive summation of feature maps at target locations [6] fails due to *target occlusion*: when a foreground finger crosses a background finger, their projections overlap. Without explicit 3D handling, features would mix erroneously, or background features might obscure the foreground. To resolve this trajectory conflict, we propose a 3D-based weighting mechanism. It acts as a differentiable Z-buffer, dynamically assigning higher importance to joints closer to the camera during feature propagation.

For each frame t , we generate target Gaussian heatmaps $\mathbf{M}_{i,t} \in \mathbb{R}^{H \times W}$ centered at the projected joint locations $\mathbf{u}_{i,t}$, and retrieve their corresponding disparity values $d_{i,t}$. We compute a dense attention weight map $\mathbf{A}_{i,t}(\mathbf{x})$ for each joint i at pixel \mathbf{x} , modulating spatial heatmap intensity with depth information:

$$\mathbf{A}_{i,t}(\mathbf{x}) = \text{softmax}_i(\log(\mathbf{M}_{i,t}(\mathbf{x}) + \epsilon) + \lambda \cdot d_{i,t}), \quad (4)$$

where λ is a learnable scaling factor that controls the sharpness of the depth prioritization. The logarithmic term ensures that the base influence is determined by spatial proximity, while the linear disparity term boosts the logits for foreground joints. Consequently, at pixels where multiple joints overlap, the softmax allocates the majority of the weight to the joint closest to the camera.

The final motion-conditioned feature map $\mathcal{F}_{motion}(\mathbf{x}, t)$ is obtained by the weighted summation of the source features:

$$\mathcal{F}_{motion}(\mathbf{x}, t) = \underbrace{\left(\sum_{i=1}^N \mathbf{A}_{i,t}(\mathbf{x}) \cdot \mathbf{f}_i \right)}_{\text{Normalized Feature}} \cdot \underbrace{\left(\sum_{j=1}^N \mathbf{M}_{j,t}(\mathbf{x}) \right)}_{\text{Total Opacity}}. \quad (5)$$

The normalization ensures features are convex combinations of joints, while the final opacity term masks out background regions where no joints are present, to ensure the purified motion guidance.

Finally, we integrate these propagated features into the video generation process. We first compress the motion feature volume \mathcal{F}_{motion} in the time dimension for matching the VAE latent following [6], then explicitly inject it into the image-to-video condition tensor \mathbf{y} of the generation model. Specifically, for all subsequent frames $t > 0$, we populate the channels of \mathbf{y} with our occlusion-aware motion features, while preserving the reference image features at $t = 0$.

3D Geometric Embeddings. While the occlusion-aware propagation ensures that visual textures are correctly mapped to target locations, relying solely on propagated visual features is still insufficient. Visual features are inherently 2D representations: the 3D-to-2D projection inevitably compresses geometric information and obscures semantic identities of different articulations. To compensate these, we introduce a secondary control stream that explicitly injects 3D information into the generation process offered by 3D spatial coordinates (u, v, d) , and distinct semantic definitions for each index of sparse 3D hand joints.

For each joint i at frame t , we construct a high-dimensional embedding $\mathbf{z}_{i,t}$ that fuses its spatial location with its semantic identity. We employ sinusoidal positional encodings $\gamma(\cdot)$ to map the projected 3D coordinates (2D position $\mathbf{u}_{i,t}$ and disparity $d_{i,t}$) into a continuous frequency domain, and concatenate this with a learnable joint identity embedding $\mathbf{E}_{id}[i]$:

$$\mathbf{z}_{i,t} = \phi([\gamma(\mathbf{u}_{i,t}, d_{i,t}); \mathbf{E}_{id}[i]]), \quad (6)$$

where $\phi(\cdot)$ is a shallow MLP projector. This indicates that the model explicitly knows which part of the hand resides at which 3D depth.

To align these sparse joint embeddings with the video latent space, we splat them onto the spatial feature grid using the previously computed Gaussian heatmaps $\mathbf{M}_{i,t}$. This creates a dense geometric map $\mathcal{F}_{geo}(\mathbf{x}, t)$ at each pixel:

$$\mathcal{F}_{geo}(\mathbf{x}, t) = \sum_{i=1}^N \mathbf{M}_{i,t}(\mathbf{x}) \cdot \mathbf{z}_{i,t}. \quad (7)$$

We concatenate the geometric map \mathcal{F}_{geo} and the motion cues \mathcal{F}_{motion} to construct the final geometric embeddings. To enforce temporal consistency, respect the causal nature of video generation, while matching the distribution of the VAE latent, we process this volume via a causal 3D convolutional head:

$$\mathcal{C}_{geo} = \text{LayerNorm}(\text{Conv3D}_{causal}([\mathcal{F}_{geo}; \mathcal{F}_{motion}])). \quad (8)$$

The causal convolution applies asymmetric padding along the time dimension, ensuring that the geometric guidance for the current frame is aggregated by historical context without leaking information from future frames.

To drive the video generation, we construct a comprehensive input for the video transformer. We concatenate the geometric control volume \mathcal{C}_{geo} with the noisy video latent \mathcal{X} and the visual condition tensor \mathbf{y} (which contains the

reference image features and motion-injected channels) along the channel dimension. Crucially, unlike computationally expensive ControlNet-like counterparts [32, 33, 63] that introduce significant overhead and risk destabilizing the pre-trained latent distribution, our strategy is lightweight ($\sim 20k$ parameters) while minimizing interference with the original latent space structure, allowing to achieve high-fidelity video quality and precise 3D control accuracy with negligible parameter cost.

3.3 Training and Inference

We build our framework upon the state-of-the-art image-to-video model WAN 2.1 [46]. To efficiently adapt the pre-trained backbone to egocentric motion control, we employ Low-Rank Adaptation (LoRA) [18] with rank $r = 64$ applied to the transformer layers. Other parameters introduced in the motion control module are trained from scratch. The entire framework is trained on our large-scale egocentric data (Section 4) on 16 NVIDIA GH200 GPUs for ~ 48 hours.

To ensure the framework’s robustness against imperfect control signals, we implement a stochastic joint masking strategy. During training, we randomly mask 5% of the input hand joints, setting all their coordinates to zero. Consequently, the model acquires the ability to plausibly generate missing articulations, ensuring temporal consistency when the upstream tracker suffers from intermittent failures or users provide sparse input during interactive editing.

During inference, the explicit nature of the 3D joint representation offers superior flexibility compared to prior methods. Our framework supports two distinct control modes: (1) Sequence Driven, where the video is driven by full trajectory sequences, and (2) Interactive Editing, where users intuitively define trajectories by dragging a single joint (or a subset of joints). In the latter mode, our model leverages its learned geometric priors to generate plausible articulation dynamics following the user-defined guidance (Section 5.2).

For domain adaptation in robotic data, although it encompasses two distinct robotic hand embodiments featuring different structural topologies and joint configurations (*i.e.*, G1-Dex3-1 and H1-Inspire), we successfully finetune a single, unified model capable of fine-grained control across both types. This highlights the strong cross-embodiment generalization capability of our framework. This flexibility is primarily attributed to our representation choice: by conditioning directly on sparse 3D joint coordinates rather than relying on embodiment-specific kinematic templates or pose priors, our control signal remains inherently embodiment-agnostic. Furthermore, by effectively resolving complex spatial interactions via our occlusion-aware conditioning and explicitly injecting structural cues through 3D geometric embeddings, the model learns universally applicable geometric priors rather than overfitting to a specific hand structure. During the finetuning phase, the model is trained for a single epoch on the mixed-embodiment video data. We jointly optimize the proposed lightweight control module and the diffusion backbone via Low-Rank Adaptation (LoRA) with a rank of $r = 64$. The entire finetuning process is highly efficient, requiring approximately 5 hours on a single node equipped with 4 NVIDIA GH200 GPUs.

4 Dataset Construction

4.1 Human Hand Data

We adopt the Ego4D [12] dataset as the large-scale video corpus for our egocentric video generation framework, which requires precise and temporally coherent hand joints to serve as control signals. Given the absence of 3D hand joint annotations in Ego4D, we propose an automated, scalable pipeline with high-fidelity hand pose extraction, spatiotemporal refinement, and quality assurance.

Hand Pose Extraction. To address severe motion blur, rapid camera movement, and frequent occlusions of unconstrained egocentric footage, we employ a decoupled frame-by-frame reconstruction paradigm. Initially, each video frame is processed by a YOLO-based detector [38] to extract tight hand bounding boxes and categorical handedness signals (left or right). These localized image crops are subsequently input into WiLoR [35], a state-of-the-art framework for in-the-wild 3D hand reconstruction, to predict MANO parameters [40], global root orientation, and camera translation.

Spatiotemporal Refinement. To synthesize temporally continuous control signals necessary for video generation, independent frame-wise predictions must be resolved into consistent tracks. This is particularly challenging in egocentric scenarios due to complex hand-object interactions and occlusions. We formulate the tracking objective as a bipartite matching problem in two primary topological slots, denoted $S \in \{L, R\}$. In each frame t , we compute an assignment cost matrix \mathbf{C} between current detections $h_i^{(t)}$ and established track slots S_j , integrating spatial continuity and semantic priors by:

$$\mathbf{C}_{i,j} = \|\mathbf{T}_i^{(t)} - \mathbf{T}_j^{(t-1)}\|_2 + \lambda \mathbb{1}(p_i^{(t)} \neq c_j), \quad (9)$$

where $\mathbf{T}_i^{(t)}$ represents the 3D global translation of the detected hand, $\mathbf{T}_j^{(t-1)}$ is the last known spatial coordinate of the track S_j , $p_i^{(t)}$ is the localized handedness, c_j is the nominal class of the slot, and $\lambda = 0.05$ penalizes handedness mismatch.

To mitigate track flickering and identity inversions during close-proximity hand interactions, we introduce a temporal hysteresis threshold τ_{swap} . A track swap is strictly prohibited unless the spatial cost improvement satisfies $\Delta\mathbf{C} > \tau_{swap}$. Furthermore, we incorporate a deterministic gap-reset mechanism: if a tracked entity is occluded for a temporal window exceeding $\tau_{gap} = 10$ frames, the track history is flushed. This effectively prevents erroneous long-distance spatial snapping upon the re-emergence of the hand.

Quality Assurance. Generative models exhibit high sensitivity to stochastic noise in control conditions, necessitating rigorous quality assurance. We therefore filter the candidate sequences by discarding video clips where valid hand instances appear in fewer than 20% of the frames, or valid MANO configurations fall below a 5% density threshold. We further eliminate sequences where more than two hands are detected for over 25% of the sequence duration. After filtering, we obtain approximately 1 million high-quality video clips. Figure 3 presents qualitative examples of our pipeline’s joint annotations projected into



Fig. 3: Qualitative results of our data annotations. The last two images are zoomed in for clear visualization of hand tracking accuracy.

2D image space. By leveraging this automated processing pipeline, we can efficiently generate large-scale, high-fidelity hand trajectory annotations.

For high-quality tracks after filtering, the optimized MANO parameters are mapped to 3D joint coordinates via the forward kinematic function:

$$\mathbf{J} = \mathcal{W}(\mathcal{M}(\boldsymbol{\theta}, \boldsymbol{\beta}), \mathbf{R}_{root}, \mathbf{T}), \quad (10)$$

where \mathcal{M} represents the MANO mesh topology defined by the pose vector $\boldsymbol{\theta}$ and the shape vector $\boldsymbol{\beta}$, which produces 3D joints $\mathbf{J} \in \mathbb{R}^{21 \times 3}$ each hand after the application of the global root rotation \mathbf{R}_{root} and translation \mathbf{T} . All extracted right-hand joints are geometrically mirrored across the sagittal (X) axis, effectively homogenizing the generative conditioning space.

4.2 Robot Hand Data

The first bottleneck in motion-controllable robotic video generation is the complete absence of datasets pairing high-fidelity egocentric robotic video with precisely aligned 3D hand trajectories in the camera coordinate system. To bridge this critical gap, we construct a robust data generation pipeline on top of Humanoid Everyday [66], which targets the Unitree H1 (Inspire hand) and G1 (DEX3-1 hand) humanoid platforms. To the best of our knowledge, we are the first to align dexterous robotic hand trajectories within the egocentric visual domain and leverage these representations as driving signals for video generation.

Achieving this alignment is non-trivial due to a confluence of compounding factors: inherent kinematic noise from the raw telemetry, ambiguities in the dimensions of the physical robots compared to their idealized CAD models (exacerbated by our restriction to offline data), and the unknown extrinsic registration between the robot’s head-mounted camera and its kinematic base frame.

Forward Kinematics in the Robot Frame. For a given physical episode, we first extract the complete joint state configuration $\mathbf{q}_t \in \mathbb{R}^D$ at each discrete timestamp t , where D denotes the total degrees of freedom of the robotic platform. We utilize the MuJoCo physics engine to compute the forward kinematics function $\mathcal{F}(\cdot)$, which maps the joint space configurations to the 3D Cartesian coordinates of the hand joints in the robot’s root frame:

$$\mathbf{P}_w^{(t)} = \mathcal{F}(\mathbf{q}_t), \quad (11)$$

where $\mathbf{P}_w^{(t)} \in \mathbb{R}^{3 \times N}$ represents the 3D positions of the N key hand joints (*e.g.*, $N = 12$ per side for the Inspire hand, and $N = 7$ for the DEX3-1 hand).

Extrinsic Parameter Optimization via Human Annotation. The most severe challenge lies in accurately transforming these 3D joints from the robot root frame \mathbf{P}_w to the egocentric camera coordinate system \mathbf{P}_c . We define the camera extrinsic transformation via a rotation matrix $\mathbf{R} \in SO(3)$ and a translation vector $\mathbf{t} \in \mathbb{R}^3$, parameterized as a 6-DoF vector $\Theta = [\theta_{pitch}, \theta_{yaw}, \theta_{roll}, t_x, t_y, t_z]^T$.

Relying solely on default CAD models invariably yields catastrophic reprojection errors. This divergence is caused by physical manufacturing tolerances, dynamic sensor mounting variations during operation, and the inherent opacity of utilizing offline data without physical access to the original hardware for traditional checkerboard calibration. To overcome the lack of reliable CAD priors, we introduce a targeted, human-in-the-loop annotation procedure. Annotators identify the ground-truth 2D pixel locations $\mathbf{u}_j^* \in \mathbb{R}^2$ of specific hand joints j across a sparsely sampled set of highly diverse frames \mathcal{A} .

We formulate the extrinsic calibration as a non-linear least-squares optimization problem, minimizing the 2D reprojection error between the human-annotated pixels and the projected kinematic joints:

$$\mathcal{L}(\Theta) = \sum_{j \in \mathcal{A}} \left\| \mathbf{u}_j^* - \pi(\mathbf{R}(\theta_{pitch}, \theta_{yaw}, \theta_{roll})\mathbf{p}_{w,j} + \mathbf{t}(t_x, t_y, t_z), \mathbf{K}) \right\|_2^2. \quad (12)$$

Here, \mathbf{K} is the known intrinsic matrix of the head-mounted camera, and $\pi : \mathbb{R}^3 \rightarrow \mathbb{R}^2$ denotes the perspective projection operator:

$$\pi([X_c, Y_c, Z_c]^T, \mathbf{K}) = \begin{bmatrix} f_x \frac{X_c}{Z_c} + c_x \\ f_y \frac{Y_c}{Z_c} + c_y \end{bmatrix}, \quad (13)$$

where f_x, f_y are the focal lengths and c_x, c_y represent the principal point coordinates. This optimization is solved using the Trust Region Reflective (TRF) algorithm. Crucially, we enforce physical bounding constraints on Θ to guarantee that the optimized camera pose converges to a solution that remains mechanically plausible, filtering out local minima caused by 2D ambiguities.

Egocentric Camera Projection. Upon converging on the optimal extrinsic parameters Θ^* for a given platform, we apply the learned transformation universally across all frames within the scene. For every frame t and every joint $i \in \{1, \dots, N\}$, the 3D camera-frame coordinates are computed as:

$$\mathbf{p}_{c,i}^{(t)} = \mathbf{R}^* \mathbf{p}_{w,i}^{(t)} + \mathbf{t}^*. \quad (14)$$

Training Video Clip Extraction. To construct the final dataset for video generation task, we extract temporally centered clips from each raw episode based on hand visibility. We define a frame’s visibility score as the total number of annotated keypoints (aggregated across both hands and wrists) with valid pixel projections within the image boundaries. To ensure temporal stability, this visibility sequence is smoothed using a moving-average filter of size 5. The

center of each clip is then anchored to the valid frame exhibiting the maximum smoothed visibility. A frame qualifies as a valid center only if it accommodates a full 121-frame temporal window (spanning 60 frames on either side) and its raw visibility count satisfies a predefined threshold. We prioritize a strict primary threshold of 8 visible keypoints, progressively relaxing it to fallback thresholds of 4, 2, or 0 only when necessary. Once anchored, the 121-frame RGB sequence is encoded into a 30 fps MP4 video. Crucially, all synchronized annotations including 3D joint coordinates, handedness labels, camera intrinsics, and frame indices are meticulously paired with the video clip.

Despite severe initial discrepancies in the raw offline telemetry, this automated batch-projection pipeline yields precise, motion-aligned egocentric trajectories. These refined trajectories successfully bridge the gap between abstract robot kinematics and the 2D visual plane, serving as the foundational control signals for our framework. In total, this rigorous processing yields a robust robotic dataset comprising 2,022 video clips for the G1-Dex3-1 embodiment and 3,486 clips for the H1-Inspire embodiment.

5 Experiments

5.1 Experimental Setup

Evaluation Datasets. To comprehensively assess our method’s generative capabilities and control accuracy, we construct evaluation splits from two distinct egocentric video benchmarks. For in-domain evaluation, we utilize the Ego4D dataset [12], a massive-scale collection of various egocentric activities in daily life. To assess out-of-domain generalization, we employ the EgoDex dataset [17]. This benchmark specifically focuses on diverse, dexterous tabletop manipulations that serve as critical priors for robotic visual-motor control. In total, the evaluation suite consists of 40 unseen video sequences from Ego4D and 30 sequences from EgoDex. These test clips are randomly sampled to ensure a diverse representation of challenging, real-world interactions, encompassing scenarios such as kitchen activities, fine-grained tabletop manipulation, and dynamic tool usage. For the evaluation in robotic field, we randomly sample 20 unseen video sequences for each of the two robotic embodiments (G1-Dex3-1 and H1-Inspire). To ensure a fair comparison and rigorously assess cross-embodiment generalization, all baseline models are finetuned for an identical duration of one epoch, matching the exact training protocol used for our framework.

Metrics. To evaluate the fidelity of generated videos, we report standard video quality metrics, including FID [16], FVD [45], PSNR, and SSIM [54]. To assess the accuracy of the generated hand motions, we use WiLoR [35] to extract 3D hands from the predicted and ground truth videos in the camera coordinate and report the procrustes-aligned Mean Per-Joint Position Error (MPJPE). We further evaluate 3D hand shape accuracy using Mean Per-Vertex Position Error (MPVPE) over all hand mesh vertices. Unlike human hand generation, where off-the-shelf pose estimators can easily extract structural keypoints, there currently exists no general-purpose method for predicting the 3D joint positions

of diverse robotic hands directly from monocular video. Consequently, directly measuring 3D tracking accuracy via explicit geometric metrics (such as MPJPE) is currently infeasible in this domain. To address this, we rely on comprehensive visual quality metrics namely FID, FVD, PSNR, and SSIM to serve as indirect proxies for tracking accuracy. Because the generated videos are explicitly conditioned on the same underlying 3D joint trajectories as the ground truth, high perceptual and temporal similarity strongly correlates with accurate motion execution. For example, if a baseline method fails to accurately track a specific finger joint during a grasping motion, it will likely generate structurally distorted hands or misaligned hand-object interactions. These severe appearance-level artifacts and temporal inconsistencies naturally diverge from the ground truth distribution, and are therefore heavily penalized by metrics like FID and FVD. Thus, by reporting these four metrics across both robot types, we can effectively benchmark both the visual fidelity and the implicit spatial control capabilities.

Baselines. We compare our method with representative approaches covering mask-based, pose-based, and track-based control paradigms. Mask2IV [24] adopts interaction masks as explicit control signals. We evaluate its second stage only, where the video diffusion model is conditioned on per-frame interaction masks. Two variants are reported: Mask2IV(H), which conditions on hand masks only, and Mask2IV(HO), which additionally incorporates object masks with ground-truth trajectories. WAN-Fun [32], built upon ControlNet [63], enables pose-guided video generation. We finetune WAN-Fun on our dataset using projected 2D hand skeletons as control inputs. For track-based control, we include WAN-Move [6] and MotionStream [43], two recent state-of-the-art methods. For WAN-Move, we report results from both the original pre-trained model and a version trained on our dataset, denoted as WAN-Move*. As the official implementation of MotionStream is not publicly released, we re-implement its architecture and train it under the same settings on our dataset for a fair comparison.

5.2 Evaluation in Human Domain

Quantitative Results. Table 1 presents the quantitative comparisons with respect to visual fidelity and 3D hand trajectory accuracy. Mask2IV, which attempts to constrain hand motion solely through 2D masks, suffers from significant visual clutter and depth ambiguity, yielding inferior results. WAN-Fun, a widely adopted pose-based baseline, is hindered by topological ambiguities inherent to 2D skeleton projections. Consequently, it falls behind our approach, showing a 14% worse FVD and a 19% higher MPJPE on the Ego4D dataset. Consistent performance gaps are observed on the EgoDex dataset, despite its relatively simpler interactions and cleaner backgrounds. When evaluated against recent state-of-the-art track-based methods MotionStream and WAN-Move* (training WAN-Move in egocentric data provides slight gains in video quality and negligible effects in hand accuracy), our explicit 3D joint-based approach achieves significantly better performance. By explicitly resolving occlusion ambiguities and injecting 3D geometric priors, our method achieves at least a 16% reduc-

Table 1: Quantitative comparisons. We evaluate performance on Ego4D [12] and EgoDex [17] datasets using visual quality metrics (FID, FVD, PSNR, SSIM) and hand control precision metrics (MPJPE, MPVPE) (**Best** , **second-best** , and **third-best**).

Method	Ego4D						EgoDex					
	Visual Quality			3D Hand Accuracy			Visual Quality			3D Hand Accuracy		
	FID ↓	FVD ↓	PSNR ↑	SSIM ↑	MPJPE ↓	MPVPE ↓	FID ↓	FVD ↓	PSNR ↑	SSIM ↑	MPJPE ↓	MPVPE ↓
Mask2IV(H) [24]	106.14	675.15	10.50	0.271	17.10	4.49	93.74	516.84	19.63	0.764	7.63	2.10
Mask2IV(HO) [24]	107.85	637.77	10.50	0.277	16.46	5.16	96.63	520.77	19.57	0.765	7.64	2.16
WAN-Fun [32]	77.39	303.54	15.68	0.436	1.76	1.78	39.92	178.67	24.55	0.842	1.85	1.88
MotionStream [43]	87.48	308.63	14.65	0.400	9.99	3.28	61.39	288.90	21.50	0.790	5.76	2.11
WAN-Move [6]	88.78	452.40	14.10	0.387	9.11	4.35	57.13	292.40	22.42	0.808	5.21	2.23
WAN-Move* [6]	88.90	332.44	14.37	0.380	9.77	4.59	52.31	316.87	23.39	0.822	5.71	2.04
Ours	67.70	259.99	15.86	0.443	1.42	1.70	39.62	174.73	24.74	0.846	1.80	1.82

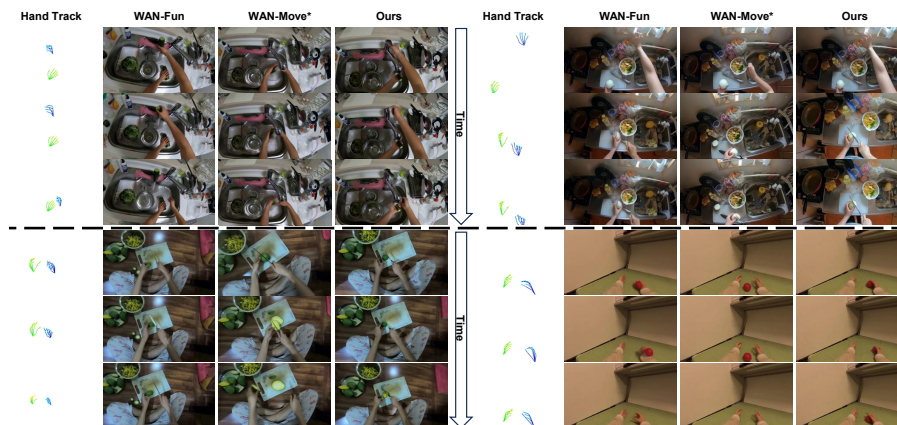


Fig. 5: Qualitative comparisons. Compared with state-of-the-art WAN-Fun [32] and WAN-Move* [6], our method shows better video quality with accurate hand control.

tion in FVD (against MotionStream on Ego4D) and a 68% reduction in MPJPE (against WAN-Move* on EgoDex).

Additionally, we present a Two-Alternative Forced Choice (2AFC) user study following [6], as detailed in Figure 4. Based on evaluations from 30 participants across 30 diverse video sequences (15 sampled from each dataset), our method significantly outperforms current state-of-the-art competitors in both perceived video quality and human-evaluated motion accuracy.

Motion Control Comparisons. As

shown in Figure 5, given a reference hand track sequence, our method con-

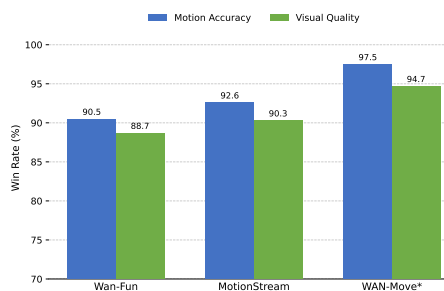


Fig. 4: The user study win rates.

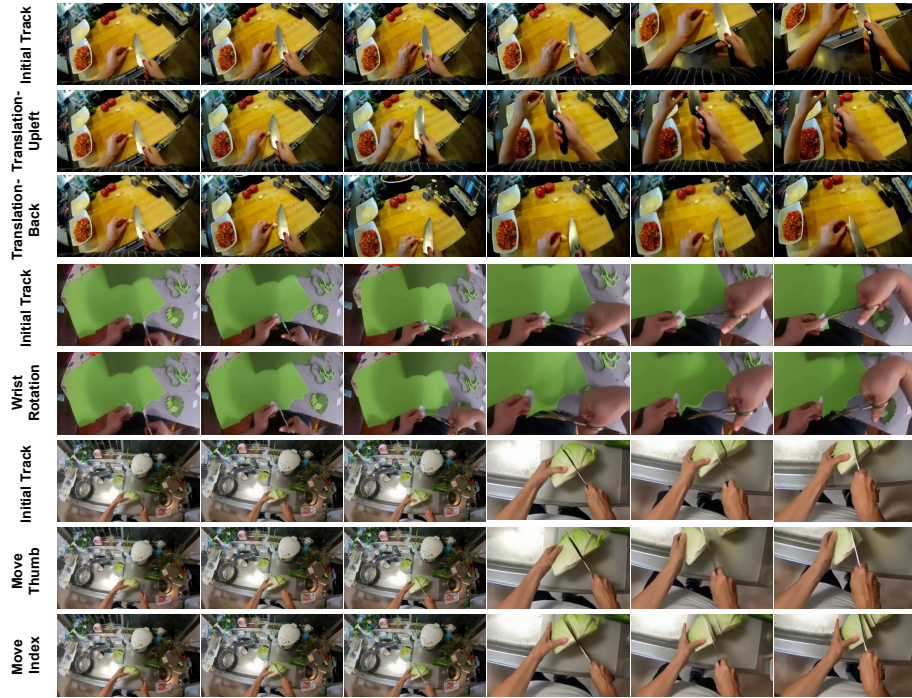


Fig. 6: Interactive fine-grained hand control results. For the bottom five rows, the last three frames are zoomed in to show subtle hand changes.

sistently outperforms the state-of-the-art pose-based WAN-Fun [32] and track-based WAN-Move* [6] in both visual fidelity and motion control accuracy. WAN-Fun frequently generates physically implausible interactions due to its limited spatial understanding of fine-grained hand articulations. For example, in the top-left scenario, the model hallucinates a detached cucumber instead of accurately grasping the faucet to control the water flow. Similarly, in the bottom-left example, it fails to execute the mango-cutting action due to poor spatial grounding of the hand trajectory. WAN-Move* demonstrates generally weaker control authority, suffering from significant spatial drift because it relies solely on unstructured 2D point tracks. As highlighted in the bottom-right example, although it captures coarse 2D translation, it inherently neglects 3D hand rotation, a critical signal for complex interactions like manipulating a ball. In contrast, our 3D-joint-based conditioning ensures precise, geometrically consistent manipulations without structural hallucinations.

Interactive Fine-Grained Control. Enabled by the spatial grounding of the sparse 3D joints, our framework naturally supports interactive video editing. We develop an intuitive user interface that allows users to seamlessly modify hand trajectories by dragging single or multiple key joints in 3D space. As shown in Figure 6, our method achieves highly accurate, fine-grained control across

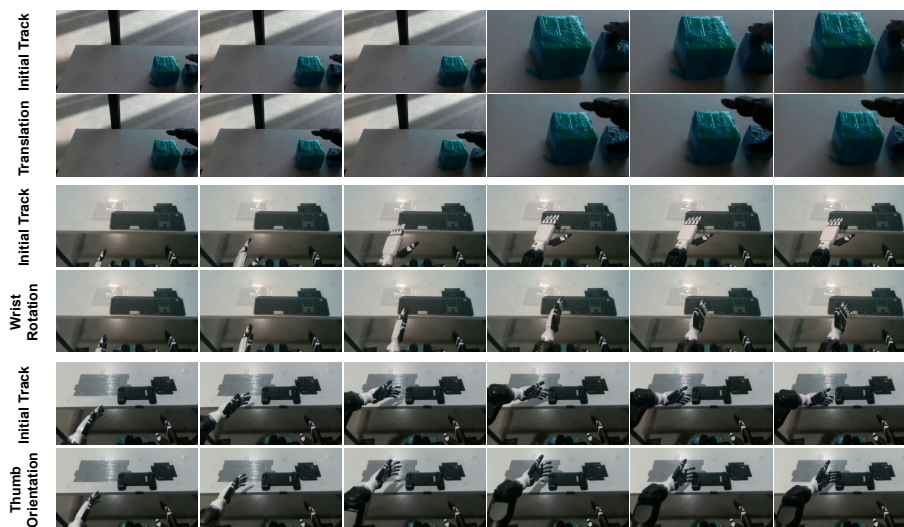


Fig. 7: Interactive control results on diverse robotic hands. Similar to our findings in the human domain, our framework effectively generalizes to robotic scenarios, enabling interactive, fine-grained dexterous control across completely different structural topologies using a single, unified fine-tuned model. The last three frames in the first two rows are cropped and magnified for enhanced visualization.

various levels of movement, ranging from macro-adjustments, such as global hand translations and complex wrist rotations, to isolated micro-manipulations, such as moving a single digit (*e.g.*, the thumb or index finger) while maintaining the structural integrity of the rest of the hand.

Furthermore, we provide additional results in the Supplementary Material demonstrating our control framework’s cross-embodiment capabilities after fine-tuning on small-scale robotic dexterous hand data. A critical advantage of using 3D hand joints as the sole control modality is its inherent morphological invariance. Unlike rigid skeletal representations or implicit poses that strictly assume human-specific kinematic chains, bone lengths, and degrees of freedom, sparse 3D joints provide a purely spatial and kinematic-agnostic control signal [36,60].

5.3 Evaluation in Robotic Domain

Qualitative Results. Figure 7 presents our interactive, fine-grained control applied to robotic scenarios. Crucially, these complex manipulations across entirely different robotic structures (G1-Dex3-1 and H1-Inspire) are achieved using a single, unified model. This demonstrates our framework’s embodiment-agnostic generalization, proving that our 3D joint conditioning successfully learns universal geometric priors rather than overfitting to a specific hand topology.

Mirroring our success in the human domain, the model maintains high-fidelity visual generation and strict geometric adherence even when executing highly

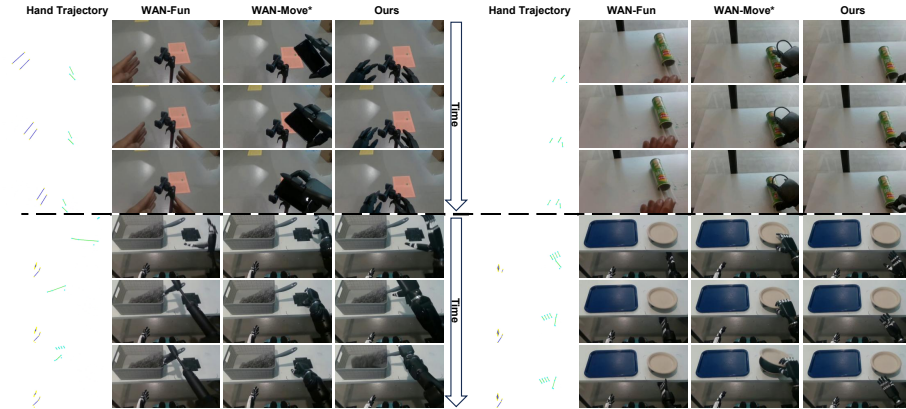


Fig. 8: Qualitative comparisons on robotic datasets. With only a single epoch of finetuning, our method achieves highly accurate control over robotic hand trajectories while seamlessly adapting to new embodiments with high visual fidelity. Conversely, under the identical finetuning protocol, WAN-Fun exhibits poor generalization due to its rigid, human-centric pose representation, while WAN-Move* demonstrates weak controllability due to the spatial ambiguity inherent in 2D tracks.

localized, subtle edits. We highlight three interaction scenarios driven by our intuitive user interface. In the first scenario, a user intuitively drags the 3D joints to globally translate the G1-Dex3-1 hand, smoothly redirecting its trajectory to interact with a completely different package. In the second example, the user applies to flip and rotate the wrist of an H1-Inspire hand as it approaches a keyboard. The model executes this out-of-plane rotation flawlessly while preserving the robot’s structural integrity. Finally, the third scene showcases isolated micro-manipulation. As the H1-Inspire hand attempts to grasp a gamepad, the user explicitly drags the thumb orientation upward. The model seamlessly isolates and articulates this single digit without distorting the rest of the grasping pose.

Figure 8 presents qualitative comparisons against WAN-Fun and WAN-Move* on our robotic test set. WAN-Fun severely struggles to generalize to new embodiments due to the intrinsic limitations of its pose representation. Because it relies on a pre-defined human skeletal topology, it cannot effectively transfer to the robotic domain after minimal finetuning, resulting in a severe degradation of trajectory controllability. For instance, as seen in the upper block, WAN-Fun frequently blends human skin textures with robotic components, yielding visually jarring and anatomically implausible artifacts. Furthermore, it fails to preserve the distinct architectural structure of the robots, severely distorting their rigid shapes (bottom-left). On the other hand, while 2D point tracks are theoretically embodiment-agnostic, WAN-Move* still exhibits weak control authority due to the critical absence of explicit 3D geometric information. Without depth awareness, it struggles to execute complex spatial manipulations. As shown in the bottom-right example, the generated robotic hand is incorrectly flipped and

Table 2: Quantitative comparisons on Humanoid Everyday [66]. We evaluate controlled video generation performance across two robot embodiment splits (G1-Dex3-1 and H1-Inspire) using visual quality metrics (FID, FVD, PSNR, SSIM). Formatting indicates **Best**, **second-best**, and **third-best** results.

Method	G1-Dex3-1				H1-Inspire			
	FID ↓	FVD ↓	PSNR ↑	SSIM ↑	FID ↓	FVD ↓	PSNR ↑	SSIM ↑
WAN-Fun [32]	65.48	272.53	22.40	0.855	55.78	349.19	20.40	0.788
MotionStream [43]	80.23	395.25	20.47	0.830	68.45	451.36	19.29	0.774
WAN-Move* [6]	82.84	388.68	20.37	0.842	67.03	446.63	19.21	0.797
Ours	50.96	187.83	24.56	0.889	37.23	226.73	23.10	0.854

spatially mispositioned. Similarly, in the bottom-left scenario, it completely fails to grasp the cleaning tool due to inaccurate trajectory grounding. In contrast, our explicit 3D joint-based framework excels in both spatial accuracy and structural preservation across different robotic embodiments.

Quantitative Results. Table 2 presents the quantitative evaluations on the robotic datasets. The results demonstrate the significant advantage of our explicit 3D joint representation when migrating to entirely new kinematic embodiments. Most notably, the performance margin by which our method outperforms the baselines is substantially amplified in the robotic domain compared to the human hand datasets.

For instance, when evaluated against the pose-based WAN-Fun, our framework achieved an FVD improvement of 2.2% on EgoDex and 14.3% on Ego4D. Strikingly, this performance gap widens dramatically to 31.1% on the G1-Dex3-1 test scenes and 35.1% on the H1-Inspire scenes. This substantial divergence indicates that methods relying on human-centric pose priors fundamentally struggle to adapt to novel kinematic structures. Their rigid skeletal topologies become a bottleneck when transferred to robots. In contrast, our embodiment-agnostic 3D joint conditioning successfully transfers geometric understanding without relying on predefined skeletal templates.

Similar performance trends are observed when evaluating against the track-based methods, MotionStream and WAN-Move*. While our method outperformed MotionStream by a maximum FVD margin of 39.5% on the human EgoDex dataset, this gap drastically expands to 52.6% on the G1-Dex3-1 robotic dataset. Likewise, our FVD lead over WAN-Move* increases from 44.8% (EgoDex) to 51.6% (G1-Dex3-1). Because track-based methods collapse 3D geometry into ambiguous 2D signals, they severely lack the spatial grounding required to accurately render the complex, unfamiliar volumes of robotic manipulators under severe occlusion. Together, these metrics quantitatively validate that our occlusion-aware, 3D geometry-preserving framework provides a highly robust and scalable control paradigm across diverse physical embodiments.

Table 3: Ablation study of key components. We sequentially analyze the contribution of Occlusion-Removed Context Aggregation (OCA), Occlusion-Aware Propagation (OP), and 3D Geometric Embeddings (3DGE) on Ego4D [12] and EgoDex [17].

Components			Ego4D					EgoDex						
OCA	OP	3DGE	FID ↓	FVD ↓	PSNR ↑	SSIM ↑	MPJPE ↓	MPVPE ↓	FID ↓	FVD ↓	PSNR ↑	SSIM ↑	MPJPE ↓	MPVPE ↓
✓			80.14	305.49	14.97	0.405	2.75	2.81	41.05	198.86	23.62	0.822	1.94	1.99
✓	✓		76.08	300.99	15.28	0.417	2.10	2.27	40.27	190.01	24.18	0.839	1.89	1.86
✓	✓	✓	67.70	259.99	15.86	0.443	1.42	1.70	39.62	174.73	24.74	0.846	1.80	1.82

5.4 Ablation Studies

Table 3 presents a quantitative analysis of the key components comprising our occlusion-aware 3D hand conditioning strategy. We establish our baseline by applying Occlusion-Removed Context Aggregation (OCA), which filters out contaminated visual features from occluded regions in the source frame. Applying this mechanism alone already yields substantial improvements in both visual quality and trajectory adherence compared to the recent state-of-the-art 2D track-based method [6]. Building upon OCA, the introduction of Occlusion-Aware Propagation (OP) addresses target occlusion ambiguities during dynamic interactions, achieving a further 5% enhancement in FID and a 23% reduction in MPJPE on the Ego4D dataset, with consistent performance gains observed on EgoDex. Finally, we demonstrate that injecting explicit 3D geometric and semantic priors is vital to achieving true 3D-aware trajectory conditioning. 3D Geometric Embeddings (3DGE) further boosts visual quality by 11% (FID) and improves structural control accuracy by 32% (MPJPE) on Ego4D.

6 Conclusion

This paper proposes a novel, lightweight framework for high-fidelity, motion-controlled video generation in egocentric scenarios. By leveraging sparse 3D hand joints as explicit control signals, our approach overcomes the limitations of 2D tracks and implicit pose representations, which frequently fail to capture precise dexterous manipulations under mutual occlusion. We introduce an occlusion-aware 3D conditioning strategy that penalizes unreliable source signals and propagates features using a 3D-based weighting mechanism towards target frames. Coupled with the direct injection of 3D geometric embeddings, our method ensures robust structural consistency while minimally disrupting the generative priors of the pre-trained backbone. Additionally, we contribute a large-scale automated annotation pipeline for the Ego4D dataset, yielding over one million high-quality clips with accurate hand trajectories. Extensive experiments validate that our method achieves superior accuracy in controlling complex egocentric interactions compared to existing baselines. Looking ahead, because the explicit representation of sparse 3D joints inherently possesses cross-embodiment characteristics, we intend to explore more applications in dexterous hand simulation for robotic tasks in the future.

Acknowledgements

We would like to thank colleagues and peers who had important advice and help on the development of the project: Zhenyu Zhao, Guanlong Jiao, Alexey Gavryushin, and Nao Wu.

References

1. Ali, A., Bai, J., Bala, M., Balaji, Y., Blakeman, A., Cai, T., Cao, J., Cao, T., Cha, E., Chao, Y.W., et al.: World simulation with video foundation models for physical ai. arXiv preprint arXiv:2511.00062 (2025) [1](#)
2. Bagchi, A., Bao, Z., Bharadhwaj, H., Wang, Y.X., Tokmakov, P., Hebert, M.: Walk through paintings: Egocentric world models from internet priors. arXiv preprint arXiv:2601.15284 (2026) [5](#)
3. Bi, H., Tan, H., Xie, S., Wang, Z., Huang, S., Liu, H., Zhao, R., Feng, Y., Xiang, C., Rong, Y., Zhao, H., Liu, H., Su, Z., Ma, L., Su, H.: Motus: A unified latent action world model. arXiv preprint arXiv:2512.13030 (2025) [5](#)
4. Blattmann, A., Dockhorn, T., Kulal, S., Mendelevitch, D., Kilian, M., Lorenz, D., Levi, Y., English, Z., Voleti, V., Letts, A., et al.: Stable video diffusion: Scaling latent video diffusion models to large datasets. arXiv preprint arXiv:2311.15127 (2023) [1](#), [4](#)
5. Burgert, R., Xu, Y., Xian, W., Pilarski, O., Clausen, P., He, M., Ma, L., Deng, Y., Li, L., Mousavi, M., Ryoo, M., Debevec, P., Yu, N.: Go-with-the-flow: Motion-controllable video diffusion models using real-time warped noise. In: CVPR (2025) [4](#)
6. Chu, R., He, Y., Chen, Z., Zhang, S., Xu, X., Xia, B., Wang, D., Yi, H., Liu, X., Zhao, H., et al.: Wan-move: Motion-controllable video generation via latent trajectory guidance. In: NeurIPS (2025) [2](#), [4](#), [6](#), [7](#), [8](#), [14](#), [15](#), [16](#), [19](#), [20](#)
7. Fu, X., Liu, X., Wang, X., Peng, S., Xia, M., Shi, X., Yuan, Z., Wan, P., Zhang, D., Lin, D.: 3dtrajmaster: Mastering 3d trajectory for multi-entity motion in video generation. In: ICLR (2024) [4](#)
8. Fung, P., Bachrach, Y., Celikyilmaz, A., Chaudhuri, K., Chen, D., Chung, W., Dupoux, E., Gong, H., Jégou, H., Lazaric, A., et al.: Embodied ai agents: Modeling the world. arXiv preprint arXiv:2506.22355 (2025) [5](#)
9. Gao, S., Liang, W., Zheng, K., Malik, A., Ye, S., Yu, S., Tseng, W.C., Dong, Y., Mo, K., Lin, C.H., Ma, Q., Nah, S., et al.: Dreamdojo: A generalist robot world model from large-scale human videos. arXiv preprint arXiv:2602.06949 (2026) [5](#)
10. Geng, D., Herrmann, C., Hur, J., Cole, F., Zhang, S., Pfaff, T., Lopez-Guevara, T., Aytar, Y., Rubinstein, M., Sun, C., et al.: Motion prompting: Controlling video generation with motion trajectories. In: CVPR. pp. 1–12 (2025) [2](#)
11. Geng, D., Herrmann, C., Hur, J., Cole, F., Zhang, S., Pfaff, T., Lopez-Guevara, T., Aytar, Y., Rubinstein, M., Sun, C., et al.: Motion prompting: Controlling video generation with motion trajectories. In: CVPR (2025) [2](#), [4](#)
12. Grauman, K., Westbury, A., Byrne, E., Chavis, Z., Furnari, A., Girdhar, R., Hamburger, J., Jiang, H., Liu, M., Liu, X., et al.: Ego4d: Around the world in 3,000 hours of egocentric video. In: CVPR. pp. 18995–19012 (2022) [4](#), [10](#), [13](#), [15](#), [20](#)
13. Hafner, D., Yan, W., Lillicrap, T.: Training agents inside of scalable world models. arXiv preprint arXiv:2509.24527 (2025) [5](#)

14. Han, X., Zhu, X., Deng, J., Song, Y.Z., Xiang, T.: Controllable person image synthesis with pose-constrained latent diffusion. In: ICCV. pp. 22768–22777 (2023) [2](#)
15. Hassan, M., Stapf, S., Rahimi, A., Rezende, P., Haghghi, Y., Brüggemann, D., Katircioglu, I., Zhang, L., Chen, X., Saha, S.: Gem: A generalizable ego-vision multimodal world model for fine-grained ego-motion, object dynamics, and scene composition control. In: CVPR. pp. 22404–22415 (2025) [4](#), [5](#)
16. Heusel, M., Ramsauer, H., Unterthiner, T., Nessler, B., Hochreiter, S.: Gans trained by a two time-scale update rule converge to a local nash equilibrium. *Advances in neural information processing systems* **30** (2017) [13](#)
17. Hoque, R., Huang, P., Yoon, D.J., Sivapurapu, M., Zhang, J.: Egodex: Learning dexterous manipulation from large-scale egocentric video. arXiv preprint arXiv:2505.11709 (2025) [4](#), [13](#), [15](#), [20](#)
18. Hu, E.J., Shen, Y., Wallis, P., Allen-Zhu, Z., Li, Y., Wang, S., Wang, L., Chen, W., et al.: Lora: Low-rank adaptation of large language models. In: ICLR (2022) [9](#)
19. Jain, Y., Nasery, A., Vineet, V., Behl, H.: Peekaboo: Interactive video generation via masked-diffusion. In: CVPR (2024) [4](#)
20. Jiang, Y., Huang, S., Xue, S., Zhao, Y., Cen, J., Leng, S., Li, K., Guo, J., Wang, K., Chen, M., Wang, F., Zhao, D., Li, X.: Rynnvla-001: Using human demonstrations to improve robot manipulation. arXiv preprint arXiv:2509.15212 (2025) [5](#)
21. Jin, Y., Sun, Z., Li, N., Xu, K., Jiang, H., Zhuang, N., Huang, Q., Song, Y., Mu, Y., Lin, Z.: Pyramidal flow matching for efficient video generative modeling. In: ICLR (2025) [1](#)
22. Kong, W., Tian, Q., Zhang, Z., Min, R., Dai, Z., Zhou, J., Xiong, J., Li, X., Wu, B., Zhang, J., et al.: Hunyuanvideo: A systematic framework for large video generative models. arXiv preprint arXiv:2412.03603 (2024) [4](#)
23. Lee, Y.C., Zhang, Z., Huang, J., Wang, J.H., Lee, J.Y., Huang, J.B., Shechtman, E., Li, Z.: Generative video motion editing with 3d point tracks. arXiv preprint arXiv:2512.02015 (2025) [2](#)
24. Li, G., Zhao, B., Yang, J., Sevilla-Lara, L.: Mask2iv: Interaction-centric video generation via mask trajectories. arXiv preprint arXiv:2510.03135 (2025) [2](#), [14](#), [15](#)
25. Li, Q., Xing, Z., Wang, R., Zhang, H., Dai, Q., Wu, Z.: Magicmotion: Controllable video generation with dense-to-sparse trajectory guidance. arXiv preprint arXiv:2503.16421 (2025) [4](#)
26. Li, Y., Wang, X., Zhang, Z., Wang, Z., Yuan, Z., Xie, L., Shan, Y., Zou, Y.: Image conductor: Precision control for interactive video synthesis. In: AAAI (2025) [4](#)
27. Lykov, A., Sam, J., Nguyen, H.K., Kozlovskiy, V., Mahmoud, Y., Serpiva, V., Cabrera, M.A., Konenkov, M., Tsetserukou, D.: Physicalagent: Towards general cognitive robotics with foundation world models. arXiv preprint arXiv:2509.13903 (2025) [5](#)
28. Ma, W.D.K., Lewis, J.P., Kleijn, W.B.: Trailblazer: Trajectory control for diffusion-based video generation. In: ACM SIGGRAPH Asia (2024) [4](#)
29. Mendonca, R., Bahl, S., Pathak, D.: Structured world models from human videos. arXiv preprint arXiv:2308.10901 (2023) [5](#)
30. Namekata, K., Bahmani, S., Wu, Z., Kant, Y., Gilitschenski, I., Lindell, D.B.: Sg-iv: Self-guided trajectory control in image-to-video generation. In: ICLR (2025) [4](#)
31. Ni, C., Zhao, G., Wang, X., Zhu, Z., Qin, W., Huang, G., Liu, C., Chen, Y., Wang, Y., Zhang, X., Zhan, Y., Zhan, K., Jia, P., Lang, X., Wang, X., Mei, W.:

- Recondreamer: Crafting world models for driving scene reconstruction via online restoration. arXiv preprint arXiv:2411.19548 (2024) 5
32. PAI, A.: Wan2.1-fun control video generation models. HuggingFace Model Collection (2025), <https://huggingface.co/collections/alibaba-pai/wan21-fun-v11> 2, 9, 14, 15, 16, 19
 33. Pallotta, E., Azar, S.M., Doorenbos, L., Ozsoy, S., Iqbal, U., Gall, J.: Egocontrol: Controllable egocentric video generation via 3d full-body poses. arXiv preprint arXiv:2511.18173 (2025) 2, 5, 9
 34. Peebles, W., Xie, S.: Scalable diffusion models with transformers. In: ICCV. pp. 4195–4205 (2023) 4
 35. Potamias, R.A., Zhang, J., Deng, J., Zafeiriou, S.: Wilor: End-to-end 3d hand localization and reconstruction in-the-wild. In: Proceedings of the Computer Vision and Pattern Recognition Conference. pp. 12242–12254 (2025) 10, 13
 36. Qin, Y., Wu, Y.H., Liu, S., Jiang, H., Yang, R., Fu, Y., Wang, X.: Dexmv: Imitation learning for dexterous manipulation from human videos. In: European Conference on Computer Vision. pp. 570–587. Springer (2022) 3, 17
 37. Qiu, H., Chen, Z., Wang, Z., He, Y., Xia, M., Liu, Z.: Freetraj: Tuning-free trajectory control in video diffusion models. arXiv preprint arXiv:2406.16863 (2024) 4
 38. Redmon, J., Farhadi, A.: Yolov3: An incremental improvement. arXiv preprint arXiv:1804.02767 (2018) 10
 39. Rombach, R., Blattmann, A., Lorenz, D., Esser, P., Ommer, B.: High-resolution image synthesis with latent diffusion models. In: CVPR. pp. 10684–10695 (2022) 4
 40. Romero, J., Tzionas, D., Black, M.J.: Embodied hands: Modeling and capturing hands and bodies together. arXiv preprint arXiv:2201.02610 (2022) 10
 41. Shi, M., Peng, S., Chen, J., Jiang, H., Li, Y., Huang, D., Luo, P., Li, H., Chen, L.: Egohumanoid: Unlocking in-the-wild loco-manipulation with robot-free egocentric demonstration. arXiv preprint arXiv:2602.10106 (2026) 5
 42. Shi, X., Huang, Z., Wang, F.Y., Bian, W., Li, D., Zhang, Y., Zhang, M., Cheung, K.C., See, S., Qin, H., et al.: Motion-i2v: Consistent and controllable image-to-video generation with explicit motion modeling. In: ACM SIGGRAPH (2024) 4
 43. Shin, J., Li, Z., Zhang, R., Zhu, J.Y., Park, J., Shechtman, E., Huang, X.: Motion-stream: Real-time video generation with interactive motion controls. arXiv preprint arXiv:2511.01266 (2025) 2, 4, 6, 14, 15, 19
 44. Tu, Y., Luo, H., Chen, X., Bai, X., Wang, F., Zhao, H.: Playerone: Egocentric world simulator. arXiv preprint arXiv:2506.09995 (2025) 2, 5
 45. Unterthiner, T., Van Steenkiste, S., Kurach, K., Marinier, R., Michalski, M., Gelly, S.: Fvd: A new metric for video generation (2019) 13
 46. Wan, T., Wang, A., Ai, B., Wen, B., Mao, C., Xie, C.W., Chen, D., Yu, F., Zhao, H., Yang, J., et al.: Wan: Open and advanced large-scale video generative models. arXiv preprint arXiv:2503.20314 (2025) 1, 4, 5, 9
 47. Wang, A., Huang, H., Fang, J.Z., Yang, Y., Ma, C.: Ati: Any trajectory instruction for controllable video generation. arXiv preprint arXiv:2505.22944 (2025) 4
 48. Wang, B., Wang, X., Ni, C., Zhao, G., Yang, Z., Zhu, Z., Zhang, M., Zhou, Y., Chen, X., Huang, G., Liu, L., Wang, X.: Humandreamer: Generating controllable human-motion videos via decoupled generation. arXiv preprint arXiv:2503.24026 (2025) 5
 49. Wang, Q., Luo, Y., Shi, X., Jia, X., Lu, H., Xue, T., Wang, X., Wan, P., Zhang, D., Gai, K.: Cinemaster: A 3d-aware and controllable framework for cinematic text-to-video generation. arXiv preprint arXiv:2502.08639 (2025) 4

50. Wang, X., Yuan, H., Zhang, S., Chen, D., Wang, J., Zhang, Y., Shen, Y., Zhao, D., Zhou, J.: Videocomposer: Compositional video synthesis with motion controllability. In: NeurIPS (2023) [4](#)
51. Wang, X., Zhang, S., Qiu, H., Chu, R., Li, Z., Zhang, Y., Gao, C., Wang, Y., Shen, C., Sang, N.: Replace anyone in videos. arXiv preprint arXiv:2409.19911 (2024) [4](#)
52. Wang, Y., Wen, C., Guo, H., Peng, S., Qin, M., Bao, H., Zhou, X., Hu, R.: Precise action-to-video generation through visual action prompts. arXiv preprint arXiv:2508.13104 (2025) [5](#)
53. Wang, Y., Ouyang, W., Wei, T., Dong, Y., Shen, Z., Pan, X.: Hand2world: Autoregressive egocentric interaction generation via free-space hand gestures. arXiv preprint arXiv:2602.09600 (2026) [5](#)
54. Wang, Z., Bovik, A.C., Sheikh, H.R., Simoncelli, E.P.: Image quality assessment: from error visibility to structural similarity. IEEE transactions on image processing **13**(4), 600–612 (2004) [13](#)
55. Wang, Z., Yuan, Z., Wang, X., Li, Y., Chen, T., Xia, M., Luo, P., Shan, Y.: Motionctrl: A unified and flexible motion controller for video generation. In: ACM SIGGRAPH. pp. 1–11 (2024) [2](#), [4](#)
56. Wu, B., Zou, C., Li, C., Huang, D., Yang, F., Tan, H., Peng, J., Wu, J., Xiong, J., Jiang, J., et al.: Hunyuanvideo 1.5 technical report. arXiv preprint arXiv:2511.18870 (2025) [1](#)
57. Wu, W., Li, Z., Gu, Y., Zhao, R., He, Y., Zhang, D.J., Shou, M.Z., Li, Y., Gao, T., Zhang, D.: Draganything: Motion control for anything using entity representation. In: ECCV (2024) [4](#)
58. Xia, B., Liu, J., Zhang, Y., Peng, B., Chu, R., Wang, Y., Wu, X., Yu, B., Jia, J.: Dreamve: Unified instruction-based image and video editing. arXiv preprint arXiv:2508.06080 (2025) [4](#)
59. Xiao, Z., Ouyang, W., Zhou, Y., Yang, S., Yang, L., Si, J., Pan, X.: Trajectory attention for fine-grained video motion control. In: ICLR (2025) [2](#), [4](#)
60. Xin, C., Yu, M., Jiang, Y., Zhang, Z., Li, X.: Analyzing key objectives in human-to-robot retargeting for dexterous manipulation. IEEE Robotics and Automation Practice (2026) [3](#), [17](#)
61. Xing, J., Mai, L., Ham, C., Huang, J., Mahapatra, A., Fu, C.W., Wong, T.T., Liu, F.: Motioncanvas: Cinematic shot design with controllable image-to-video generation. In: ACM SIGGRAPH (2025) [2](#), [4](#)
62. Zhang, B., Shou, M.Z.: Ego-centric predictive model conditioned on hand trajectories. arXiv preprint arXiv:2508.19852 (2025) [5](#)
63. Zhang, L., Rao, A., Agrawala, M.: Adding conditional control to text-to-image diffusion models. In: ICCV. pp. 3836–3847 (2023) [2](#), [9](#), [14](#)
64. Zhang, W., Foo, L.G., Beeler, T., Dabral, R., Theobalt, C.: Vhoi: Controllable video generation of human-object interactions from sparse trajectories via motion densification. arXiv preprint arXiv:2512.09646 (2025) [2](#), [5](#)
65. Zhang, Z., Liao, J., Li, M., Dai, Z., Qiu, B., Zhu, S., Qin, L., Wang, W.: Tora: Trajectory-oriented diffusion transformer for video generation. In: CVPR (2025) [4](#)
66. Zhao, Z., Jing, H., Liu, X., Mao, J., Jha, A., Yang, H., Xue, R., Zakharor, S., Guizilini, V., Wang, Y.: Humanoid everyday: A comprehensive robotic dataset for open-world humanoid manipulation. arXiv preprint arXiv:2510.08807 (2025) [4](#), [11](#), [19](#)
67. Zhou, H., Wang, C., Nie, R., Liu, J., Yu, D., Yu, Q., Wang, C.: Trackgo: A flexible and efficient method for controllable video generation. In: AAAI (2025) [4](#)